Collaborative Optimization of Thermodynamic and Kinetic for Ni-based Hydroxides in Electrocatalytic Urea Oxidation Reaction

Zhicheng Zheng [a], Dan Wu [a], Long Chen [a], Shuo Chen [a], Hao Wan [b], Gen Chen [a], Ning Zhang [a], Xiaohe Liu [a, b, *], Renzhi Ma [c, *]

[a] *School of Materials Science and Engineering and School of Minerals Processing and Bioengineering, Central South University, Changsha, Hunan 410083, P. R. China.*

[b] *Zhongyuan Critical Metals Laboratory, Zhengzhou University, Zhengzhou, 450001, PR China.*

[c] *International Center for Materials Nanoarchitectonics (WPI-MANA), National Institute for Materials Science (NIMS), Namiki 1-1, Tsukuba, Ibaraki 305-0044, Japan.*

* Corresponding authors.

Email addresses: liuxh@csu.edu.cn (X. Liu), Ma.renzhi@nims.go.jp (R. Ma).

Highlights

- Co element doping in Ni hydroxide shows the best brilliant synergist effect than other transition metal elements for efficient urea oxidation reaction.

- A competitive effect between UOR and redox reaction on Ni-based hydroxides is found during anode oxidation process while UOR would restrain the redox reaction of Ni-based hydroxides.

- DFT calculation indicates the brilliant UOR performance of Ni-based hydroxides is adjusted by energy barriers of UOR RDS and redox reaction which involved with cooperation of thermodynamic and kinetic.

Abstract: Ni-based hydroxides are brilliant electrocatalysts for alkaline urea oxidation reaction (UOR). Herein, multiple Ni-based hydroxides were investigated by electrocatalytic test for UOR performance. Electrocatalytic performance of different ratios of NiCo LDHs was further determined to exploring electrochemical reaction pathway and thermodynamic mechanism. Results indicate appropriate Co element doping content in Ni hydroxide could greatly improve UOR performance. Results of XPS and in situ Raman indicate only part of NiCo hydroxides were converted to NiCo oxyhydroxides which drive the subsequent UOR. Moreover, electrocatalytic UOR on NiCo oxyhydroxides is found in competition with redox of NiCo hydroxides. Density function theory (DFT) calculation manifests that the energy barrier of UOR on NiCo oxyhydroxides is lower than redox of NiCo hydroxides which become the limitation reaction. Energy barrier gap between UOR and redox which provide driving force for UOR which is the primary cause of fast kinetic.

Graphical abstract

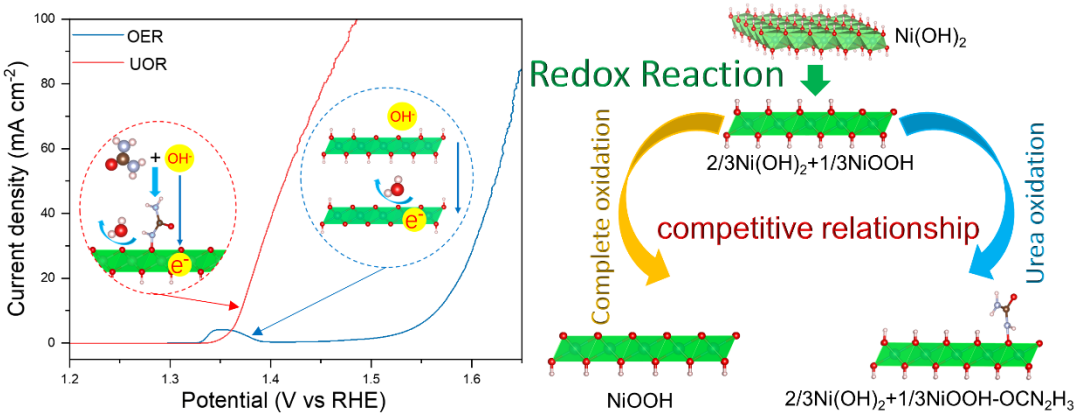

Hydroxide ions in alkaline electrolyte are essential raw materials for anodic reactions which include redox reaction, UOR and OER. A competitive relationship between consuming ions is actually formed. The first produced oxyhydroxides can strongly push the UOR forward and even quickly grab all the surrounding hydroxyl ions. As a result, the redox reaction is inhibited.

Keywords: Urea oxidation reaction; NiCo LDHs; electrocatalysis; density function theory.

1. Introduction

Energy crisis and environment protection have always been issues of widespread concern to the community[1, 2]. The development of hydrogen energy is the ideal development direction of green and clean energy[3, 4]. Electrolysis reaction is an efficient and convenient method for the conversion of electrical energy to hydrogen energy[5-7]. In water solution system, typically, hydrogen is obtained by the reduction half reaction at cathode, while the corresponding half reaction is the anodic oxidation reaction. Generally, hydrogen evolution reaction (HER) is a low thermodynamic energy barrier reaction and simple two electrons process. Under the action of industrial Pt/C catalyst, a certain HER current density could be achieved at dozens millivolt of potential[8, 9]. In the anode reaction, as an electron donor reaction, direct oxidation of water is a quite convenient option for anode reaction. However, the large thermodynamic potential (1.23 V) and complex four electrons process inevitably lead to low conversion efficiency of electric energy to hydrogen energy[10, 11]. In terms of electric conversion efficiency, many chemicals which possess low thermodynamic oxidation potential were chosen to replace direct water splitting, like small molecule alcohols and aldehydes[12, 13], monomeric sugar molecules[14] and urea[15-17]. Urea oxidation reaction (UOR), which has an extremely low thermodynamic potential (0.37 V), could be a great option for replacing water oxidation[18, 19]. Apart from hydrogen generation, UOR is also an essential reaction in direct urea fuel cells, urea-rich wastewater purification and so on[20, 21]. Hence, developing efficient and economic catalysts is critical for reducing the power consumption of UOR in energy conversion reaction.

Consider the cost of catalysts and the subsequent promotion, inexpensive and efficient catalysts are the ideal choice. Among various inexpensive catalysts, transition metal materials, include metallic, oxides, hydroxides, and their derivatives, show outstanding electrocatalytic UOR performance[22-24]. By virtue of high performance and

low-cost synthesis method, hydroxides are widely considered as the most promising catalysts for UOR as well as OER. Among all of those hydroxides, Ni-based hydroxides exhibit best efficient performance on UOR in alkaline environment as the formation of highly active Ni-based oxyhydroxides during electrochemical process[25, 26]. In the current researches, NiOOH, which transformed form Ni hydroxide at redox potential, was also considered to be the true active constituent in UOR[27]. In the subsequent UOR process, there are two pathways of indirectly urea chemical-oxidized ($6NiOOH + CO(NH_2)_2 + H_2O \rightarrow 6Ni(OH)_2 + N_2 + CO_2$) and directly urea electro-oxidized ($NiOOH\text{-}CO(NH_2)_2 + 6OH^- \rightarrow NiOOH + N_2 + CO_2 + 5H_2O + 6e^-$) into N_2 and CO_2 on the formative NiOOH[28, 29]. Interestingly, in the exiting studies, most of Ni-containing catalysts show a very close potential in UOR and redox reaction while lack of explanation[21, 29]. This phenomenon indicates UOR performance of Ni-containing catalysts have been connected to their redox reaction which is worth investigating. Therefore, investigating the relationship between UOR on oxyhydroxides and redox of hydroxides is the key breakthrough to further improve UOR performance. Moreover, after the formation of NiOOH, the specific UOR pathway and thermodynamic mechanism in alkaline electrochemical process are still unclear which seriously hinder the exploration of UOR high-performance catalysts.

Electronic state structure of catalysts is directly related to catalytic reaction process include redox of hydroxides. And the most efficient method to adjust the electronic structure of materials is impurity element doping which lead to strong electronic interaction[30, 31]. Typically, thanks to the optimization of electronic structure, the doping of Fe element in Ni and Co hydroxides have outstanding performance in OER by adjusting adsorption energy of intermediates[32, 33]. Therefore, looking for the star doping element in Ni hydroxide for UOR is the primary task. With the widespread popularity of density function theory (DFT) calculation, electronic structure of catalysts and intermediates adsorption could be simulated for investigating variety catalytic reaction in detail[34, 35]. As the structural model is flexible adjustable, DFT calculation is a reliable method to predict conversion reaction pathway and reaction preference. In

this work, multiple impurity element doping Ni-based hydroxides were synthesized systematacially for investigating the element synergy in UOR. An exact contrastive analysis of the connection between formation of Ni-based oxyhydroxides and UOR performance was conducted by electrochemical methods. Furthermore, NiCo LDHs were chosen as object of in-depth study for dissecting the true active constituent and catalytic mechanism of UOR. Density function theory (DFT) calculation was used to simulate the density of electronic states and adsorption energy of intermediates in UOR. By analyzing the results of experiment and simulation, a complete and tight mechanism of Ni-based hydroxides in UOR was proposed. This work is instructive and meaningful for mechanism investigation and development of high-performance catalysts in UOR.

2. Experimental Section

2.1. Materials

Nickel(II) chloride hydrate ($NiCl_2 \cdot 6H_2O$, Sinopharm Group Co. Ltd., China), Aluminium chloride hydrate ($AlCl_3 \cdot 6H_2O$, Sinopharm Group Co. Ltd., China), Cobalt (II) chloride hydrate ($CoCl_2 \cdot 4H_2O$, Sinopharm Group Co. Ltd., China), Chromic chloride hydrate ($CrCl_3 \cdot 6H_2O$, Sinopharm Group Co. Ltd., China), Copper chloride hydrate ($CuCl_2 \cdot 2H_2O$, Sinopharm Group Co. Ltd., China), Ferric(II) chloride hydrate ($FeCl_2 \cdot 4H_2O$, Sinopharm Group Co. Ltd., China), lithium chloride hydrate ($LiCl \cdot H_2O$, Sinopharm Group Co. Ltd., China), Magnesium chloride hydrate ($MgCl_2 \cdot 6H_2O$, Sinopharm Group Co. Ltd., China), Manganese (II) chloride hydrate ($MnCl_2 \cdot 4H_2O$, Sinopharm Group Co. Ltd., China), Zinc chloride anhydrous ($ZnCl_2$, Sinopharm Group Co. Ltd., China), Hexamethylenetetramine (HMT, Sinopharm Group Co. Ltd., China), sodium gluconate salt ($C_6H_{11}NaO_7$, Shanghai Macklin Biochemical Co. Ltd., China), nafion solution (10 wt%, Hangzhou wanengda technology Co. Ltd., China), carbon paper (TORAY, Japan), potassium hydroxide (KOH, Sinopharm Group Co. Ltd., China), urea (Sinopharm Group Co. Ltd., China).

2.2. Synthesis of samples

All of hydroxides were synthesized by one-step hydrothermal method. For the NiM (M = Al, Co, Cr, Cu, Fe, Li, Mg, Mn, Zn) hydroxides, a ratio of 9:1 in Nickel(II) chloride hydrate and other one metal chloride hydrate with a total molar quantity of 40 mmol were dissolved in 300 mL deionized water. 0.01 mmol sodium gluconate salt and 20 mmol Hexamethylenetetramine were subsequently added in previous saline solution. The mixed solution was heated at 120 ℃ for 8 h. After cooling down naturally, the precipitate was collected by centrifugation, washed 3 times with deionized water and ethanol, and eventually dried at 60 °C for 12 h. The samples were noted as NiM LDH. For the Ni_xCo_{1-x} LDH, different ratio of Nickel(II) chloride hydrate and Cobalt(II) chloride hydrate with a total molar quantity of 40 mmol were dissolved in 300 mL deionized water. The subsequent operating steps were same as synthesis steps of NiM LDH.

2.3. Materials characterization

The crystallographic composition was investigated by X-ray diffraction (XRD, Rigaku D/miniflex 600) with Cu Kα radiation (λ =1.54 Å) and 40 kV/15 mA. X-ray photoelectron spectroscopy (XPS) was recorded on a Thermo Fisher ESCALAB 250Xi spectrophotometer. The in situ Raman spectrums of $Ni_{0.864}Co_{0.136}$ LDH were collected from Horiba LabRAM HR Evolution at multiple applied voltages in 1 M KOH with and without 0.5 M urea.

2.4. Electrochemical measurements

Electrochemical measurements were obtained on a CHI 760E electrochemical analyzer (CH Instruments, Inc., Shanghai) in a standard three-electrode system. 5 mg as-prepared catalyst was dissolved into 1 mL of the mixed solution of ethanol and deionized water (volume ratio is 1:1), and then 20 μL 10 wt% Nafion aqueous solution was added. The suspension was dispersed by ultrasound for 30 min to obtain a

homogeneous ink. 100 μL of ink was uniformly dropped on carbon fiber paper with an exposure area of 1 cm^2. Hg/HgO electrode and carbon rod as reference and counter electrodes, respectively. Unless otherwise noted, potentials in this study were calibrated with respect to the reversible hydrogen electrode (RHE) scale according to the following equation:

$$E_{RHE} = E_{(Hg/HgO)} + 0.098\ V + 0.059 \times pH - i_{(Hg/HgO)} \times R_s$$

Where pH values of electrolytes were listed in **Table S1**. 40 cycles of cyclic voltammetry (CV) scan with a scan rate of 30 mV s^{-1} were used to activate the catalysts in 1 M KOH. The polarization curves were measured after activation in 1 M KOH aqueous solution with and without 0.5 M urea at room temperature with a scan rate of 1 mV s^{-1} and iR correction which solution resistance was measured by electrochemical impedance spectroscopy (EIS). While EIS was gathered at 0.6 V vs Hg/HgO in 1 M KOH and at 0.45 V vs Hg/HgO in 1 M KOH with 0.5 M urea in the frequency range of 0.01 - 100000 Hz with an AC voltage amplitude of 5 mV. Electrochemical surface area (ECSA) was measured by cyclic voltammetry (CV) using the same working electrodes at a potential window of 0.2 - 0.3 V vs Hg/HgO (1 M KOH). CV curves were obtained at different scan rates of 10, 20, 30 … 100 mV s^{-1}. After plotting charging current density differences ($\Delta j = j_a - j_c$ at 0.25 V vs Hg/HgO, where j_a is the anode current density and j_c is the cathode current density) versus the scan rates, the slope is equal to twice of the double-layer capacitance C_{dl}. The ECSA values was calculated using equation:

$$ECSA = \frac{C_{dl}}{C_s}$$

Where C_{dl} is the electric double-layer capacitance calculated from non-Faradaic region, and C_s is the specific capacitance of black carbon paper.

2.5. Computational details for calculations

The density functional theory (DFT) calculations are performed by the Vienna Ab initio Simulation Package (VASP) with the projector augmented wave (PAW) method. Generalized gradient approximation (GGA) of Perdew-Burke-Ernzerhof (PBE)

functional is used for the exchange-functional. 20 Å of vacuum spacing in a direction perpendicular to the plane of the catalyst is used to avoid interaction between units. The Brillouin zone integration is performed using 3 × 3 × 1 Monkhorst-Pack k-point sampling for a structure. The cut-off energy of the plane-wave basis is set at 400 eV. The self-consistent calculations apply a convergence energy threshold of 10^{-4} eV. The Hubbard U (DFT + U) corrections for 3d transition metal by setting with a U-J value of 3.3 eV for Co atom and 6.2 eV for Ni atom. Single layer of hydroxide was changed into oxyhydroxide by removing partial H atoms from the model. Other intermediates adsorption models were shown in **Figure 5**f and supporting information. The vibrational frequencies were computed to consider the zero-point energies, enthalpy, and entropy and ultimately calculate the free energies at room temperature (298.15 K).

3. Results and discussion

3.1. Elements synergy analysis of Ni-based hydroxides in UOR

For investigating the reaction mechanism and synergistic effect of Ni-based hydroxides in electrocatalytic UOR, Ni hydroxide and multifarious element-doped NiM (M = Al, Co, Cr, Cu, Fe, Li, Mg, Mn, Zn) layer double hydroxides (LDH) were synthesized by one-pot hydrothermal method. Corresponding structural and morphology representation was shown in **Figure S1** and **Figure S2**, which the results indicated all of NiM LDH were successfully obtained. Linear sweep voltammetry (LSV) plots were corrected in alkaline electrolyte for measuring the OER and UOR performance. **Figure 1**a shows the LSV plots collected in 1 M KOH solution which representing OER. Obviously, the doping of Fe element has the strongest synergistic effect with Ni hydroxide in OER performance, which is far more than any other elements, and this result is consistent with most research reports[36]. When the electrolyte was replaced by 1 M KOH with 0.5 M urea, similar with the brilliant effect of Fe element in OER, Co element also has an outstanding effect in UOR performance. For 10 mA cm^{-2} current density, a potential of 1.332 V is needed for NiCo LDH in UOR

which is much lower than the potential of NiCo LDH in OER (1.545 V) even the potential of NiFe LDH in OER (1.489 V). This result gives a clear manifestation of the thermodynamic advantage of UOR in alkaline solution and the brilliant performance of Co doping in Ni hydroxide for UOR. Apart from the thermodynamic advantages, UOR has an absolute advantage in kinetic. As a whole, for all NiM LDH, the Tafel slopes (as shown in **Figure 1**c) of UOR are much lower than OER. In especially, NiCo LDH has an extremely low Tafel slope of 18.7 mV dec^{-1} in UOR, which is almost fifth of Tafel slope of OER. The results of electrochemical impedance spectra (EIS, as shown in **Figure 1**d) exhibited electron transfer of all NiM LDH in UOR. All Nyquist plots were divided into semicircle and straight line which are controlled by charge transfer and diffusion process[37], respectively. In all NiM LDH, NiCo LDH exhibited the lowest resistance (corresponding to the minimum radius of semicircle) which indicated the fastest reaction electron transfer kinetic in UOR.

Absolute thermodynamic and kinetic advantages of UOR make it in a dominant position in the competition with OER. However, recent reports show that, before OER occurs in alkaline solution, NiM LDH will turn into oxyhydroxides at a certain potential which is represented in LSV plots as redox peaks. Generally, oxyhydroxides were considered as the true active phase of OER[38]. Nevertheless, there is large potential gap between oxyhydroxide forming potential and OER onset potential. The reason is that rate-determining step in OER is adsorption and desorption of intermediates which is more difficult than the formation of oxyhydroxide. Interestingly, as the comparison results of LSV plots in OER and UOR (as shown in **Figure 1**e and **1**f), the UOR onset potentials of all NiM LDH are close to corresponding redox potentials. The amazing consistency of the two kinds of potentials indicated the difficulty of rate-determining step in UOR is similar even lower than corresponding redox potentials. And the oxyhydroxides may be still closely related to the true active phase of UOR. Therefore, further study of the relationship between UOR and oxyhydroxide is the key to explore catalytic mechanism and improve performance of Ni-based LDH.

3.2. Element ratio regulates UOR catalytic performance

As the brilliant performance in electrocatalytic UOR, NiCo LDH was choose to be the representative study subject for analyzing performance improvement mechanism of Ni-based LDH in UOR. Different ratios of NiCo LDHs were prepared and the corresponding structural characterization was exhibited in **Figure S4**. **Figure S5** shows the actual element content of NiCo LDHs. **Figure 2**a and **2**b exhibited LSV plots measured in 1 M KOH and 1 M KOH with 0.5 M urea, respectively. Same as most reports, in the OER process, arbitrary ratios of NiCo LDHs (include Ni hydroxide and Co hydroxide) show a similar performance. On the contrary, there are huge performance differences between them in UOR process. Obviously, the UOR performance of Ni hydroxide is superior to Co hydroxide. However, low-doping of Co element can greatly improve UOR performance of Ni hydroxide while overmuch-doping of Co element would degrade the performance. A low potential of 1.307 V for $Ni_{0.864}Co_{0.136}$ LDH at 10 mA cm^{-2} exhibited the optimal UOR performance among all ratios of NiCo LDHs which well below the OER potential (1.547 V) to reach the same current density. Results of Tafel slopes (as shown in **Figure 2**c) indicate that all NiCo LDHs have similar kinetics in OER while huge difference in UOR. Ni hydroxide has a faster UOR kinetics than Co hydroxide. Nonetheless, a little bit of Co doping in Ni hydroxide can significantly improve UOR kinetics, and the optimal effect was obtained at $Ni_{0.864}Co_{0.136}$ LDH. Meanwhile, the minimum circle radius of $Ni_{0.864}Co_{0.136}$ LDH in Nyquist plots indicate the fastest rate of electron transfer. Moreover, in the $Ni_{0.864}Co_{0.136}$ LDH and NiCo LDHs with lower Co content, straight line in the high frequency region manifests that UOR was controlled by diffusion in electrolyte. In other words, the electron transfer rate at electrode is far beyond requirement and the diffusion of intermediates is the key factor that hinder UOR rate.

In the same way, comparing the LSV plots of UOR and redox peak plots in 1 M KOH come to a result that all plots have a great coincidence degree. When Co content does not exceed $Ni_{0.864}Co_{0.136}$ LDH, UOR accompanied by the formation reaction of

oxyhydroxides in those NiCo LDHs which demonstrates those NiCo oxyhydroxides possess terrific UOR activity and selectivity. However, when Co content exceed $Ni_{0.864}Co_{0.136}$ LDH, there are separate redox peaks in LSV plots of NiCo LDHs. This result visually indicates the oxyhydroxides is formed before UOR occurs and oxyhydroxides are true active phase of UOR. Even so, the onset potential of UOR is obviously lower than those NiCo LDHs which Co content does not exceed $Ni_{0.864}Co_{0.136}$ LDH. This result manifest high Co-containing NiCo LDHs have a thermodynamic advantage than low Co-containing NiCo LDHs in UOR while hindered by the sluggish kinetic. The in-depth mechanism will be explained in detail in the DFT calculation. For exploring the stability of NiCo LDH catalysts, the optimal $Ni_{0.864}Co_{0.136}$ LDH was chosen to sustain UOR and OER at potential of 0.6 V vs Hg/HgO. As a whole, compared with OER, UOR current density maintain a great superiority at the same potential. The UOR current density inevitably decrease with the consumption of urea while the current density immediately restores with the refreshment of electrolyte. As shown in insert figure in **Figure 2**f, after sustaining over 35 h of UOR, $Ni_{0.864}Co_{0.136}$ LDH still maintains high activity and selectivity.

3.3. Competition mechanism of Ni-based hydroxides conversion in UOR

Hydroxide ions and urea molecules concentration-dependent experiments of $Ni_{0.864}Co_{0.136}$ LDH were carried out for further investigating the influence of electrolyte in UOR. In the single alkaline water oxidation process, hydroxide ions are the sole reactant which results in an extremely pH dependent OER process (as shown in **Figure 3**a). However, the pH dependence is not only reflected in OER but also in redox process. With the decrease of KOH concentration, redox potential has a great right shift to high voltage which verify the important role of hydroxide ions in redox of hydroxides. UOR performance of $Ni_{0.864}Co_{0.136}$ LDH still keep pace with redox as demonstrated from **Figure 3**b and **3**d. This result indicates hydroxide ions also play an important role in UOR. Moreover, Tafel slopes were increase with the decrease of hydroxide ions concentration which indicate the UOR kinetic of $Ni_{0.864}Co_{0.136}$ LDH was hindered.

However, when the concentration of urea was changed, there was little difference in the onset potential of UOR and Tafel slopes. All of those results indicate kinetic of UOR on $Ni_{0.864}Co_{0.136}$ LDH is directly subject to hydroxide ions concentration. And here is the proof of that electrolyte diffusion control reaction reflected from EIS is dominated by hydroxide ions. Furthermore, when urea concentration in electrolyte is very low (0.1 M), the decrease and fluctuation of current density are attribute to the competition failure with redox and electrocatalytic OER of $Ni_{0.864}Co_{0.136}$ LDH

XPS spectrums of $Ni_{0.864}Co_{0.136}$ LDH gathered from before and after UOR were used to investigate the evolution of NiCo LDHs during UOR. Moreover, XPS spectrums of $Ni_{0.864}Co_{0.136}$ LDH gathered after OER was gathered for comparison. As shown in **Figure 4**a, in all of the high-resolution Ni 2p spectrums of $Ni_{0.864}Co_{0.136}$ LDH, two spin-orbit doublets of Ni $2p_{1/2}$ and Ni $2p_{3/2}$ could be well fitted. Meanwhile, two separated peaks at 855.1 eV and 856.7 eV could be fitted in Ni $2p_{3/2}$ which attribute to Ni^{2+} and Ni^{3+}, respectively. **Figure 4**b exhibited the high-resolution Co 2p spectrums of $Ni_{0.864}Co_{0.136}$ LDH and two spin-orbit doublets of Co $2p_{1/2}$ and Co $2p_{3/2}$ could be well fitted. And similarly, two separated peaks at 779.5 eV and 781.1 eV could be fitted in Co $2p_{3/2}$ which attribute to Co^{3+} and Co^{2+}, respectively. Generally, the peaks area tends to present corresponding content of valence elements. In the initial $Ni_{0.864}Co_{0.136}$ LDH, the content of Ni^{3+} is 30.4 % which was oxidized during hydrothermal process. And Co element in initial $Ni_{0.864}Co_{0.136}$ LDH almost remain absolute bivalent. Evolution of catalysts is closely related to the changes of valance states. During the evolution of $Ni_{0.864}Co_{0.136}$ LDH in alkaline solution with applying voltage, emergence of trivalent Ni and Co tends to represent the formation of corresponding oxyhydroxides[39]. After sustaining 35 h of UOR and OER, the content of trivalent Ni increase to 47.8 % and 77.9 %, respectively. And the content of trivalent Co increase to 17.6 % and 36.4 %, respectively. This result indicates that more hydroxides was converted to oxyhydroxides at same potential during OER than UOR. In other words, UOR might be competing with the redox reactions and becomes dominant with the increase of applied voltage.

For investigating structural evolution of $Ni_{0.864}Co_{0.136}$ LDH in detail, in situ Raman was measured on electrode coating $Ni_{0.864}Co_{0.136}$ LDH in the processes of OER and UOR. **Figure 4**c shows the in situ Raman spectrums of $Ni_{0.864}Co_{0.136}$ LDH at voltage cycle in 1 M KOH. There are two obvious peaks at 502 cm^{-2} and 526 cm^{-2} corresponding to Ni hydroxide (as Co atoms are substitutional atoms and Ni hydroxide is major structure, Ni hydroxide and Ni oxyhydroxide could be expressed as representatives). With the increase of applied voltage, two peaks located at 470 cm^{-1} and 553 cm^{-1} consumingly emerge which corresponding to typical Ni oxyhydroxide. Moreover, the two peaks of Ni hydroxide gradually become relatively unclear at 0.5 V vs Ag/AgCl. This result indicates the great mass of Ni hydroxide turns into Ni oxyhydroxide at a high potential. However, in the Raman spectrums of $Ni_{0.864}Co_{0.136}$ LDH in 1 M KOH with 0.5 M urea, as shown in **Figure 4**d, the peaks of Ni hydroxide have been dominant throughout voltage cycling process while the peaks of Ni oxyhydroxide are slightly enhanced only at high voltage. This result indicates just a small amount of Ni hydroxide turns into Ni oxyhydroxide at a high potential. Those results have a great agreement with results of XPS. Furthermore, when the applied voltage goes from high to low, peaks of Ni oxyhydroxide gradually recover to initial state during both OER and UOR. This result manifests that the transformation of Ni hydroxide is reversible during both OER and UOR. **Figure 4**e and **3**f summarized peak intensity of the whole voltage cycle at 470 cm^{-1} and 553 cm^{-1} during OER and UOR. It is observed that peaks intensity at 470 cm^{-1} and 553 cm^{-1} reach the strongest at 0.5 V vs Ag/AgCl and rapidly decrease when voltage recovery in 1 M KOH. However, in 1 M KOH with 0.5 M urea, peaks intensity at 470 cm^{-1} and 553 cm^{-1} increases gradually when voltage exceeding 0.1 V vs Ag/AgCl and reach strongest at 0.4 V vs Ag/AgCl. This result manifests the formation of oxyhydroxides in UOR and oxyhydroxides is still the true active constituent. With the potential further increase to 0.5 V vs Ag/AgCl, the reduction of peaks intensity at 470 cm^{-1} and 553 cm^{-1} indicates that UOR and redox reaction are competitive reactions and the UOR is dominant at high potential. This slight reduction is caused by the indirectly urea chemical-oxidized pathway while the

generated hydroxides cannot be oxidized again. Moreover, the amount of oxyhydroxides formed during UOR process obviously is lower than that of OER which is agree with the results of XPS. This result indicated oxyhydroxides possess extremely high activity and selectivity for UOR.

For further explaining the mechanism of $Ni_{0.864}Co_{0.136}$ LDH in UOR on the surface of electrode in detail, a schematic diagram (as shown in **Figure 4**g) is presented. The whole process takes charge transfer as the object of analysis. First, as the voltage is applied to redox potential, $Ni_{0.864}Co_{0.136}$ LDH translate into $Ni_{0.864}Co_{0.136}$ oxyhydroxides and this process is actually deprotonation in which the charge is transferred from the hydroxide ion to the catalyst. After the formation of $Ni_{0.864}Co_{0.136}$ oxyhydroxides, the catalyzed UOR also occurs. However, the first even first four steps of UOR are all essentially deprotonation. This inevitably leads to a competitive relationship between the UOR and redox process. Obviously, the dominant UOR process in high potential takes up most of the hydroxide ions and leads to the low formation of oxyhydroxides. Moreover, from the results of EIS, there are diffusion control steps in UOR which indicate aggregation rate of the hydroxide ions cannot keep up with the UOR reaction rate. When the formed $Ni_{0.864}Co_{0.136}$ oxyhydroxides consume all of the hydroxide ions to catalyze UOR, the conversion of $Ni_{0.864}Co_{0.136}$ LDH to $Ni_{0.864}Co_{0.136}$ oxyhydroxides will be completely stopped. In this case, UOR catalyzed by $Ni_{0.864}Co_{0.136}$ oxyhydroxides must possess similar even better thermodynamic conditions than redox of $Ni_{0.864}Co_{0.136}$ LDH. Therefore, the deeper thermodynamic advantages between UOR catalyzed be $Ni_{0.864}Co_{0.136}$ oxyhydroxides and redox of $Ni_{0.864}Co_{0.136}$ LDH need to be further investigated.

3.4. UOR mechanism analysis of high-performance Ni-based hydroxides

For further investigating the mechanism of $Ni_{0.864}Co_{0.136}$ LDH in UOR, density functional theory (DFT) calculations were carried out to reveal the electronic structure and underlying thermodynamic process. The projected partial density of states (PDOSs)

of Ni and Co in Ni hydroxide, Co hydroxide and NiCo LDH are demonstrated in **Figure 5**a, **5**b and **5**c, respectively. Obviously, Ni-3d and Co-3d orbital in all of hydroxides provide major active electron around the Fermi level which act as the active site to support electron transfer. In Co hydroxide, there is a band gap of 0.54 eV around the Fermi level which shows a poor electronic activity. The Ni hydroxide is more active as the Ni-3d orbital have a PDOSs of -2.46 eV in the Fermi level. This result could explain the higher redox charge in Ni hydroxide than Co hydroxide shown in LSV plots. Moreover, when Co element is doped into Ni hydroxide, the Co-3d orbital has a considerable change which a PDOSs of -1.64 eV in Fermi level is provided. And the own Ni-3d orbital in NiCo LDH could still provide a high PDOSs of -2.51 eV in the Fermi level. Obviously, the doping of Co element could increase the electrons occupation around the Fermi lever in NiCo LDH. More electrons occupation around the Fermi level help NiCo LDH shows more active electron transfer in reaction which is agree with **Figure 2**e.

The Gibbs free energy of UOR pathways were further calculated for investigating energy barrier of Ni hydroxide, Co hydroxide and NiCo LDH in UOR. In general, the first four steps of UOR pathways are deprotonation of four hydrogen atoms in urea molecule which is followed by the release of N_2 and CO_2. As shown in **Figure 5**d, all of them have same rate-determining step that is deprotonation of the fourth hydrogen atom in urea molecule. And Ni hydroxide exhibits the lowest RDS energy barrier of 1.546 eV which confirm the best UOR performance. Moreover, Co hydroxide exhibits the highest RDS energy barrier of 1.724 eV which indicate the poor UOR performance. This result agrees with the result of electrochemical experiment well. However, the higher RDS energy barrier of NiCo LDH than Ni hydroxide is inconsistent with experimental results. This contradiction illustrates UOR performance of Ni-based hydroxides is not limited by RDS of UOR. For further investigating the limitation factor of Ni-based hydroxides during UOR, energy barriers of conversion from hydroxide to oxyhydroxides (noted as redox process) was simulated by DFT. As shown in **Figure 5**e, Ni hydroxide, Co hydroxide and NiCo LDH exhibit redox energy barrier of 1.712

eV, 1.489 eV and 1.656 eV, respectively. According to the reaction sequence of hydroxides in alkaline solution, the redox process is prior to the subsequent urea oxidation. For this matter, the limitation step of hydroxides in UOR depend on redox process if the energy barrier of redox is higher the RDS of urea oxidation. On the contrary, the RDS of urea oxidation becomes limitation step if energy barrier of redox process is lower than urea oxidation. There is evidence to support this point form the lower redox energy barrier and higher apparent UOR overpotential (as shown in **Figure 2**b) of Co hydroxide. From this perspective, despite the Co doping in Ni hydroxide improves energy barrier of RDS in urea oxidation, the higher energy barrier of redox process in NiCo LDH than RDS of urea oxidation still remain the limitation step which is the reason why Ni-based hydroxides possess such high kinetic rate of UOR. Moreover, kinetic is not only dependent on thermodynamic driving but also the number of active sites. As the results of **Figure 2**c, low Co-doping in Ni hydroxide could accelerate kinetic process of UOR. This is attribute to the enhanced competitiveness of redox reaction. As the narrowing energy barrier gap between redox reaction and UOR RDS in low Co-containing NiCo LDHs, the competitive advantage of UOR is also diminishing which means more NiCo oxyhydroxides could be formed. Absolute energy barrier gap and more active sites promote the fast kinetic of UOR. Hence, the Co doping in Ni hydroxide facilitates redox process and further leads to the optimized apparent UOR performance is combination of thermodynamic and kinetic optimization.

A comprehensive analysis of experimental results and theoretical simulation was investigated in detail and the complete mechanism of Ni-based hydroxides in alkaline UOR process was summarized clearly. As for the whole reaction process, as shown in **Figure 5**f, the Ni-based hydroxides was firstly converted to Ni-based oxyhydroxides which act the true active constituent of urea electrooxidation. And then, urea molecules were oxidized on the surface of Ni-based oxyhydroxides by multi-steps include deprotonation of four hydrogen atoms and release of gas molecules. The evolution of Ni-based hydroxides during applied voltage process was shown clearly via contact with the LSV plots. In the range 1 with low applied voltage, Ni-based hydroxides remain the

original stable structure. when the applied voltage rises up to the redox potential (in range 2), part of Ni-based hydroxides begins to translate to Ni-based oxyhydroxides. As the RDS energy barrier of UOR on the surface of Ni-based oxyhydroxides is lower than redox of Ni-based hydroxides, a large electronic driving energy to adsorb and electrolysis urea molecules was created at that potential. Hence, the formative Ni-based oxyhydroxides rapidly catalyze UOR and consume the hydroxide ions that accumulate around the electrode surface. As the amount of hydroxide ions is limited by ions migration in electrolyte, the UOR certainly will consume all of hydroxide ions once the formative Ni-based oxyhydroxides is enough. However, the redox process of Ni-based hydroxides is also a deprotonation process which need to consume hydroxide ions. And the higher energy barrier compels all of hydroxide ions to tend to participate in UOR which means the redox process of Ni-based hydroxide will be discontinued. In this case, in range 3, a low Ni-based oxyhydroxides content in Ni-based hydroxides could maintain a high current density of UOR. In other case, when there is no urea in the electrolyte, the higher OER energy barrier of Ni-based oxyhydroxides results in most of Ni-based hydroxides to form oxyhydroxides at a high potential.

4. Conclusion

In summary, multiple impurity elements doping in Ni hydroxide were synthesized and the corresponding UOR performance of NiM LDH in alkaline was determined by electrochemical measurements. It is found that the UOR overpotentials of all NiM LDH have a dependency with the corresponding redox potential. Nevertheless, the dependency is broken by comparing the UOR performance of different ratios of NiCo LDHs. Low Co element doping content in Ni hydroxide could greatly improve UOR performance while is relatively poor for high doping content even Co hydroxide. Results of XPS and in situ Raman measurements indicate the electrocatalytic UOR on NiCo oxyhydroxides is in competition with redox of NiCo hydroxides and dominant at high applied voltage. DFT calculation shows that energy barrier of UOR on NiCo

oxyhydroxides is lower than redox of NiCo hydroxides which become the limitation reaction. Co doping in Ni hydroxide could effectively reduce energy barrier of redox which is the immediate cause of improved UOR performance. energy difference between UOR RDS and redox which provide great driving force is the primary cause of fast kinetic. This work provided a theoretical and experimental support for binary and even multiple Ni-based hydroxides in electrocatalytic UOR and is instructive and meaningful for mechanism investigation and development of high-performance catalysts in UOR.

Author contribution

The manuscript was written through contributions of all authors. All authors have given approval to the final version of the manuscript.

Acknowledgements

The authors acknowledge the financial support by the National Natural Science Foundation of China (U20A20123). This work was supported in part by the High Performance Computing Center of Central South University.

Formatting of funding sources

This work was supported by the National Natural Science Foundation of China (U20A20123).

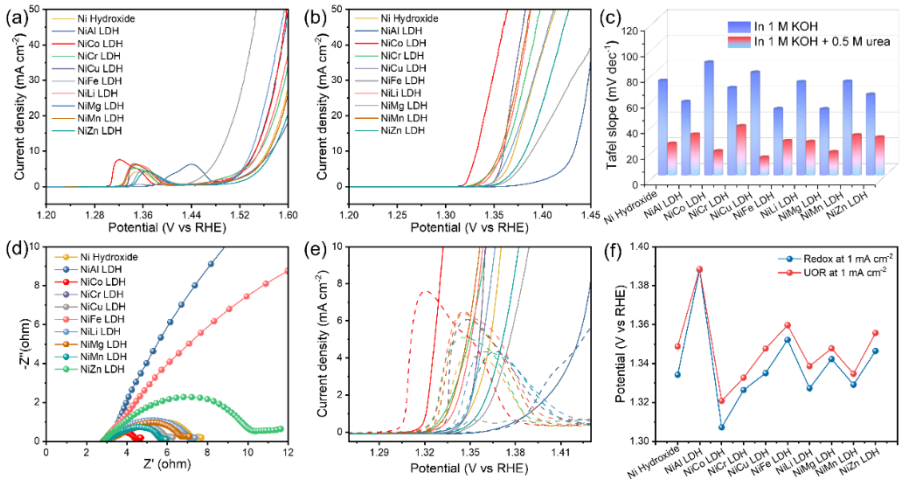

Figure 1 Electrochemical measurement results of Ni hydroxide and NiM LDH. (a) LSV plots in 1 M KOH and (b) LSV plots in 1 M KOH with 0.5 M urea; (c) Tafel slopes; (d) Nyquist plots measured at 0.45 V vs Hg/HgO in 1 M KOH with 0.5 M urea; (e) comparison chart of LSV plots of Ni hydroxide and NiM LDH in OER and UOR; (f) the potentials of Ni hydroxide and NiM LDH at 1 mA cm^{-2} in redox and UOR.

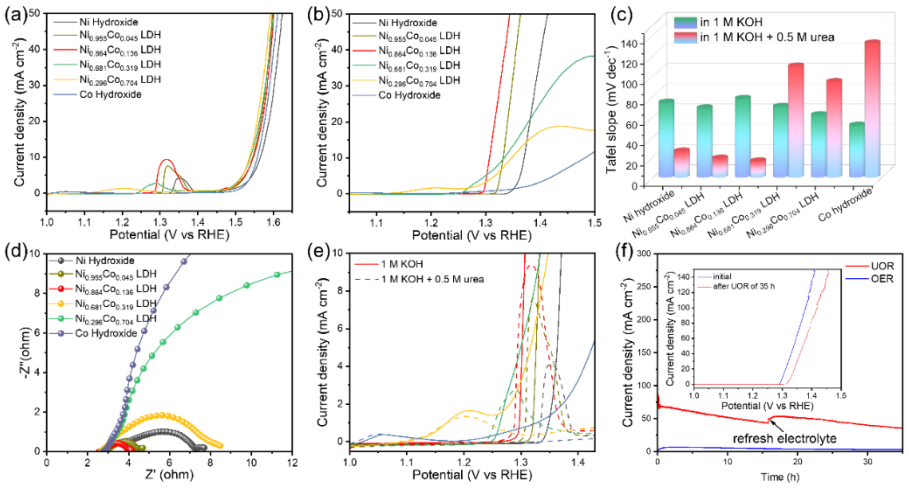

Figure 2 Electrochemical measurement results of NiCo LDHs. (a) LSV plots in 1 M KOH and (b) LSV plots in 1 M KOH with 0.5 M urea; (c) Tafel slopes; (d) Nyquist plots measured at 0.45 V vs Hg/HgO in 1 M KOH with 0.5 M urea; (e) comparison chart between redox and UOR with LSV plots of NiCo LDHs; (f) amperometric i-t curves of $Ni_{0.864}Co_{0.136}$ LDH measured in 1 M KOH with and without 0.5 M urea with a potential of 0.6 V vs Hg/HgO.

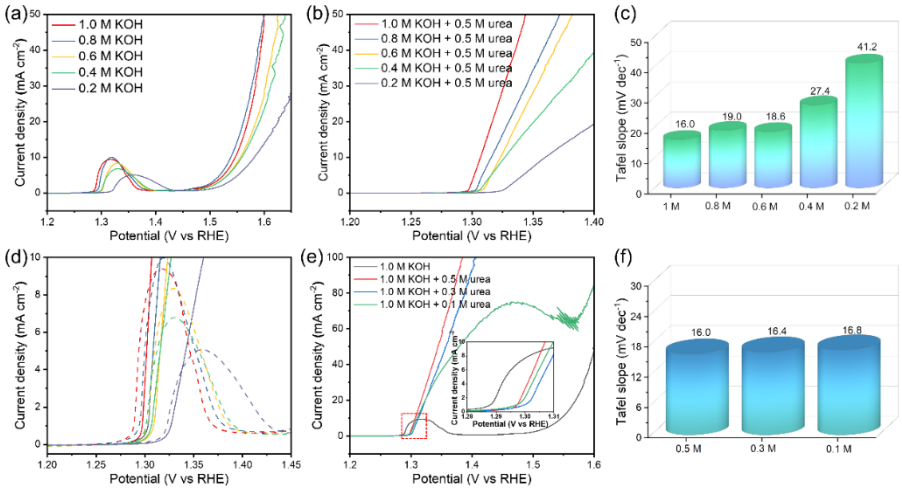

Figure 3 Hydroxide ions and urea molecules dependent experiments: (a) LSV plots of $Ni_{0.864}Co_{0.136}$ LDH in different concentration of KOH without urea; (b) LSV plots of $Ni_{0.864}Co_{0.136}$ LDH in different concentration of KOH with 0.5 M urea; (c) Tafel slopes of $Ni_{0.864}Co_{0.136}$ LDH in different concentration of KOH with 0.5 M urea; (d) comparison chart between redox and UOR with LSV plots of $Ni_{0.864}Co_{0.136}$ LDH; (e) LSV plots of $Ni_{0.864}Co_{0.136}$ LDH in 1 M KOH with different concentration of urea (insert figure shows the enlarged image of red box); (f) Tafel slopes of $Ni_{0.864}Co_{0.136}$ LDH in 1 M KOH with different concentration of urea.

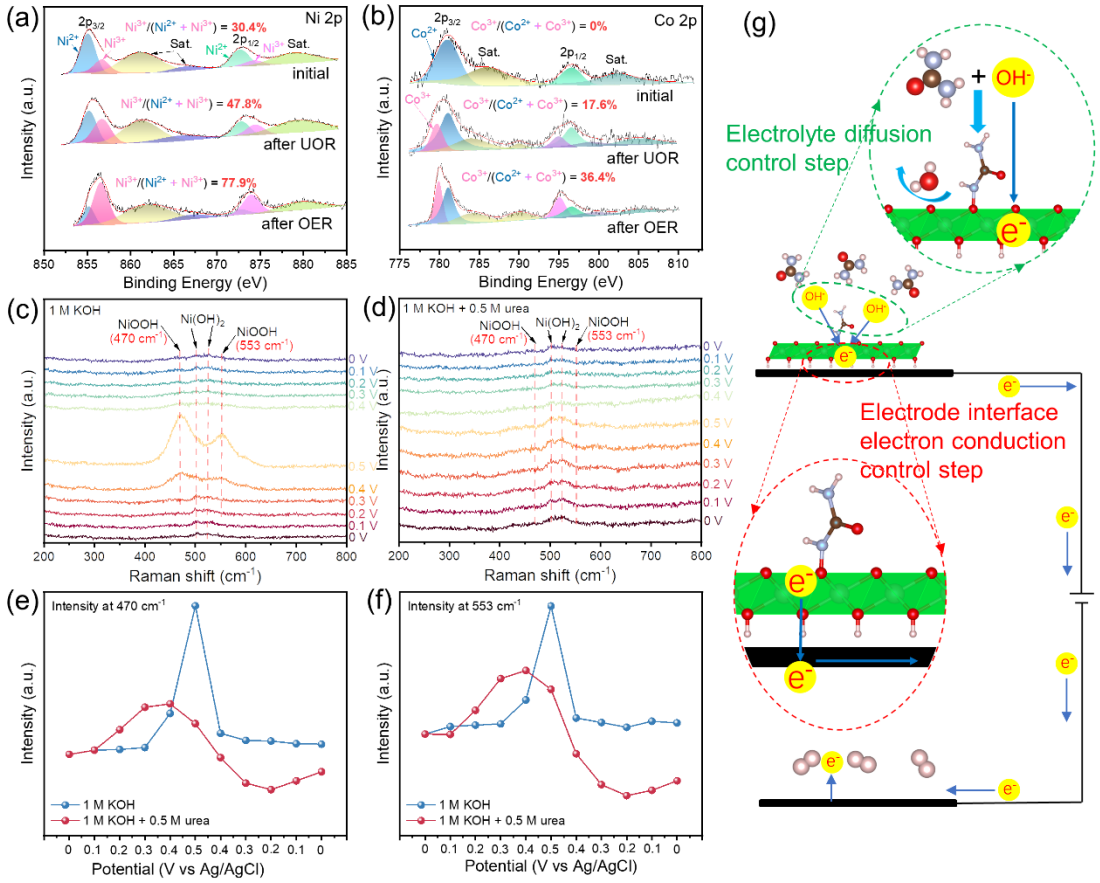

Figure 4 XPS spectrum of $Ni_{0.864}Co_{0.136}$ LDH obtained from initial powder, after 35 h of UOR and OER: (a) Ni 2p and (b) Co 2p; in situ Raman investigations on $Ni_{0.864}Co_{0.136}$ LDH with different electrolytes: (c) 1 M KOH and (d) 1 M KOH with 0.5 M urea; the peak intensity of oxyhydroxide at different potential: (e) peak at 470 cm^{-1} and (f) peak at 553 cm^{-1}; (g) the schematic diagram of electrolyte diffusion control step and electrode interface electron conduction control step.

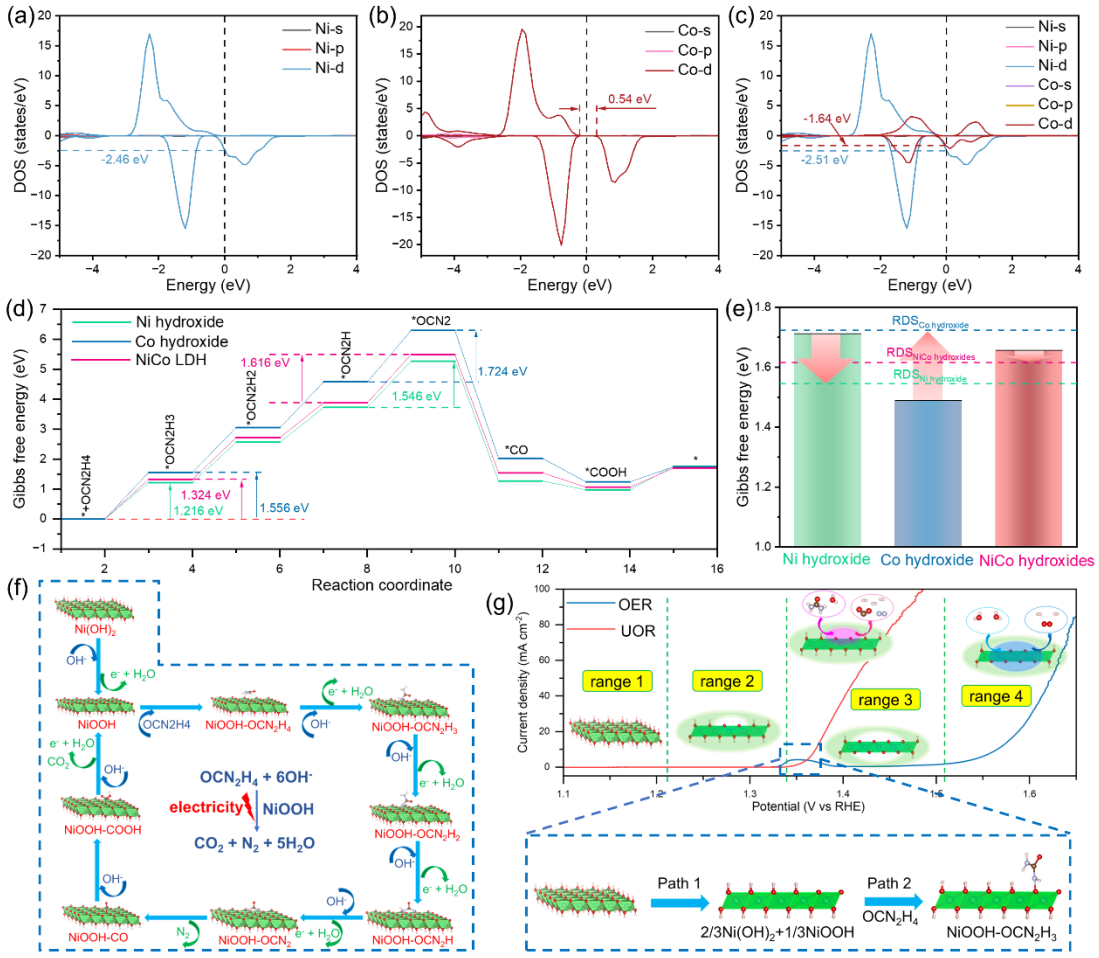

Figure 5 PDOSs of Ni and Co in (a) Ni hydroxide, (b) Co hydroxide and (c) NiCo LDH; (d) reaction coordinates free energy profiles of UOR on Ni hydroxide, Co hydroxide and NiCo LDH (all of them are treated with corresponding oxyhydroxide in UOR calculation process); (e) free energy barrier for the conversion of hydroxides to oxyhydroxides at different degrees of conversion and corresponding UOR onset energy; (f) schematic diagram of UOR process; (g) schematic diagram of catalytic process of $Ni_{0.864}Co_{0.136}$ LDH at different voltage ranges.

References

[1] J. Zhang, L. Yu, Y. Chen, X.F. Lu, S. Gao, X.W.D. Lou, Designed Formation of Double-shelled Ni-Fe layered-double-hydroxide nanocages for efficient oxygen evolution reaction, Adv. Mater. 32 (2020) e1906432. https://doi.org/10.1002/adma.201906432.

[2] P. Li, Y. Huang, X. Ouyang, W. Li, F. Li, S. Tian, Unusual hcp Ni with metal and non-metal dual doping modulation to realize boosted urea oxidation, Chem. Eng. J. 464 (2023) 142570. https://doi.org/10.1016/j.cej.2023.142570.

[3] E. Liu, J. Li, L. Jiao, H.T.T. Doan, Z. Liu, Z. Zhao, Y. Huang, K.M. Abraham, S. Mukerjee, Q. Jia, Unifying the hydrogen evolution and oxidation reactions kinetics in base by identifying the catalytic roles of hydroxyl-water-cation adducts, J. Am. Chem. Soc. 141 (2019) 3232-3239. https://doi.org/10.1021/jacs.8b13228.

[4] Z. Chen, R. Zheng, H. Zou, R. Wang, C. Huang, W. Dai, W. Wei, L. Duan, B.-J. Ni, H. Chen, Amorphous iron-doped nickel boride with facilitated structural reconstruction and dual active sites for efficient urea electrooxidation, Chem. Eng. J. 465 (2023) 142684. https://doi.org/10.1016/j.cej.2023.142684.

[5] F.Y. Yu, Z.L. Lang, L.Y. Yin, K. Feng, Y.J. Xia, H.Q. Tan, H.T. Zhu, J. Zhong, Z.H. Kang, Y.G. Li, Pt-O bond as an active site superior to Pt(0) in hydrogen evolution reaction, Nat. Commun. 11 (2020) 490. https://doi.org/10.1038/s41467-019-14274-z.

[6] L. Qiao, A. Zhu, D. Liu, J. Feng, Y. Chen, M. Chen, P. Zhou, L. Yin, R. Wu, K.W. Ng, H. Pan, Crystalline phosphides/amorphous oxides composite for energy-saving hydrogen production assisted by efficient urea oxidation reaction, Chem. Eng. J. 454 (2023) 140380. https://doi.org/10.1016/j.cej.2022.140380.

[7] X. Lin, L. Chen, X. Zhong, A. BaQais, W. Dang, M.A. Amin, H. Huang, H. Li, G. Liang, G. Liu, Z. Yang, N-doped bimetallic phosphides composite catalysts derived from metal-organic frameworks for electrocatalytic water splitting, Adv. Compos. Hybrid Mater. 6 (2023) 79. https://doi.org/10.1007/s42114-023-00660-1.

[8] Q. Yang, H. Liu, P. Yuan, Y. Jia, L. Zhuang, H. Zhang, X. Yan, G. Liu, Y. Zhao, J. Liu, S. Wei, L. Song, Q. Wu, B. Ge, L. Zhang, K. Wang, X. Wang, C.R. Chang, X. Yao, Single carbon vacancy traps atomic platinum for hydrogen evolution catalysis, J. Am. Chem. Soc. 144 (2022) 2171-2178. https://doi.org/10.1021/jacs.1c10814.

[9] Z. Zhang, X. Liu, D. Wang, H. Wan, Y. Zhang, G. Chen, N. Zhang, R. Ma, Ruthenium composited $NiCo_2O_4$ spinel nanocones with oxygen vacancies as a high-efficient bifunctional catalyst for overall water splitting, Chem. Eng. J. 446 (2022) 137037. https://doi.org/10.1016/j.cej.2022.137037.

[10] S. Anantharaj, S. Kundu, S. Noda, "The Fe effect": a review unveiling the critical roles of Fe in enhancing OER activity of Ni and Co based catalysts, Nano Energy 80 (2021) 105514. https://doi.org/10.1016/j.nanoen.2020.105514.

[11] D. Zhou, P. Li, X. Lin, A. McKinley, Y. Kuang, W. Liu, W.F. Lin, X. Sun, X. Duan, Layered double hydroxide-based electrocatalysts for the oxygen evolution reaction: identification and tailoring of active sites, and superaerophobic nanoarray

electrode assembly, Chem. Soc. Rev. 50 (2021) 8790-8817. https://doi.org/10.1039/d1cs00186h.
[12] Z. Li, M. Shao, H. An, Z. Wang, S. Xu, M. Wei, D.G. Evans, X. Duan, Fast electrosynthesis of Fe-containing layered double hydroxide arrays toward highly efficient electrocatalytic oxidation reactions, Chem. Sci. 6 (2015) 6624-6631. https://doi.org/10.1039/c5sc02417j.
[13] M. Li, X. Deng, Y. Liang, K. Xiang, D. Wu, B. Zhao, H. Yang, J.-L. Luo, X.-Z. Fu, Co P@NiCo-LDH heteronanosheet arrays as efficient bifunctional electrocatalysts for co-generation of value-added formate and hydrogen with less-energy consumption, J. Energy Chem. 50 (2020) 314-323. https://doi.org/10.1016/j.jechem.2020.03.050.
[14] W.J. Liu, Z. Xu, D. Zhao, X.Q. Pan, H.C. Li, X. Hu, Z.Y. Fan, W.K. Wang, G.H. Zhao, S. Jin, G.W. Huber, H.Q. Yu, Efficient electrochemical production of glucaric acid and H_2 via glucose electrolysis, Nat. Commun. 11 (2020) 265. https://doi.org/10.1038/s41467-019-14157-3.
[15] Y. Song, Z. Ji, S. Zhao, T. Wang, J. Liu, W. Hu, Reaction site exchange in hierarchical bimetallic Mn/Ni catalysts triggered by the electron pump effect to boost urea electrocatalytic oxidation, J. Mater. Chem. A 10 (2022) 10417-10426. https://doi.org/10.1039/d2ta01318e.
[16] Q. Zhang, F.M.D. Kazim, S. Ma, K. Qu, M. Li, Y. Wang, H. Hu, W. Cai, Z. Yang, Nitrogen dopants in nickel nanoparticles embedded carbon nanotubes promote overall urea oxidation, Appl. Catal. B-Environ. 280 (2021) 119436. https://doi.org/10.1016/j.apcatb.2020.119436.
[17] X. Xu, G. Zhang, J. Li, H. Liu, G. Su, Z. Shi, M. Huang, Redistributing interfacial charge density of $Ni_{12}P_5/Ni_3P$ via Fe doping for ultrafast urea oxidation catalysis at large current densities, Chem. Eng. J. 452 (2023) 139362. https://doi.org/10.1016/j.cej.2022.139362.
[18] D. Zhu, C. Guo, J. Liu, L. Wang, Y. Du, S.Z. Qiao, Two-dimensional metal-organic frameworks with high oxidation states for efficient electrocatalytic urea oxidation, Chem. Commun. 53 (2017) 10906-10909. https://doi.org/10.1039/c7cc06378d.
[19] M. Li, X. Wu, K. Liu, Y. Zhang, X. Jiang, D. Sun, Y. Tang, K. Huang, G. Fu, Nitrogen vacancies enriched Ce-doped Ni_3N hierarchical nanosheets triggering highly-efficient urea oxidation reaction in urea-assisted energy-saving electrolysis, J. Energy Chem. 69 (2022) 506-515. https://doi.org/10.1016/j.jechem.2022.01.031.
[20] B. Zhu, Z. Liang, R. Zou, Designing advanced catalysts for energy conversion based on uea oxidation reaction, Small 16 (2020) e1906133. https://doi.org/10.1002/smll.201906133.
[21] H. Jiang, M. Sun, S. Wu, B. Huang, C.S. Lee, W. Zhang, Oxygen-incorporated NiMoP nanotube arrays as efficient bifunctional electrocatalysts For urea-assisted energy-saving hydrogen production in alkaline electrolyte, Adv. Funct. Mater. 31 (2021) 2104951. https://doi.org/10.1002/adfm.202104951.
[22] H. Yang, M. Yuan, D. Wang, Z. Sun, H. Li, G. Sun, 3D cross-linked structure of manganese nickel phosphide ultrathin nanosheets: electronic structure

optimization for efficient bifunctional electrocatalysts, ACS Appl. Energy Mater. 4 (2021) 8563-8571. https://doi.org/10.1021/acsaem.1c01756.
[23] X. Jia, H. Kang, X. Yang, Y. Li, K. Cui, X. Wu, W. Qin, G. Wu, Amorphous Ni(Ⅲ)-based sulfides as bifunctional water and urea oxidation anode electrocatalysts for hydrogen generation from urea-containing water, Appl. Catal. B Environ. 312 (2022) 121389. https://doi.org/10.1016/j.apcatb.2022.121389.
[24] X. Liu, K. Ni, B. Wen, R. Guo, C. Niu, J. Meng, Q. Li, P. Wu, Y. Zhu, X. Wu, L. Mai, Deep reconstruction of nickel-based precatalysts for water oxidation catalysis, ACS Energy Lett. 4 (2019) 2585-2592. https://doi.org/10.1021/acsenergylett.9b01922.
[25] H. Zhang, X. Meng, J. Zhang, Y. Huang, Hierarchical NiFe hydroxide/Ni_3N nanosheet-on-nanosheet heterostructures for bifunctional oxygen evolution and urea oxidation reactions, ACS Sustain. Chem. Eng. 9 (2021) 12584-12590. https://doi.org/10.1021/acssuschemeng.1c03353.
[26] J. Xie, W. Liu, X. Zhang, Y. Guo, L. Gao, F. Lei, B. Tang, Y. Xie, Constructing hierarchical wire-on-sheet nanoarrays in phase-regulated cerium-doped nickel hydroxide for promoted urea electro-oxidation, ACS Mater. Lett. 1 (2019) 103-110. https://doi.org/10.1021/acsmaterialslett.9b00124.
[27] D. Li, Y. Zhang, X. Zhou, C. Huang, Y. Wen, L. LIu, Q. Li, Y. Xu, Y. Wu, Q. Ruan, Y. Ma, F. Xiong, D. Xiao, P. Liu, G. Wang, B. Mehrjou, H. Li, R. Chen, H. Ni, Z. Zeng, P.k. Chu, Dynamic active sites on plasma engraved Ni hydroxide for enhanced electro-catalytic urea oxidation, J. Energy Chem. 71 (2022) 150-158. https://doi.org/10.1016/j.jechem.2022.03.040.
[28] H. Liu, S. Zhu, Z. Cui, Z. Li, S. Wu, Y. Liang, Ni_2P nanoflakes for the high-performing urea oxidation reaction: linking active sites to a UOR mechanism, Nanoscale 13 (2021) 1759-1769. https://doi.org/10.1039/d0nr08025j.
[29] X. Zhu, X. Dou, J. Dai, X. An, Y. Guo, L. Zhang, S. Tao, J. Zhao, W. Chu, X.C. Zeng, C. Wu, Y. Xie, Metallic nickel hydroxide nanosheets give superior electrocatalytic oxidation of urea for fuel cells, Angew. Chem. Int. Ed. 55 (2016) 12465-12469. https://doi.org/10.1002/anie.201606313.
[30] K. Gao, B. Wang, L. Tao, B.V. Cunning, Z. Zhang, S. Wang, R.S. Ruoff, L. Qu, Efficient metal-free electrocatalysts from N-doped carbon nanomaterials: mono-doping and Co-doping, Adv. Mater. 31 (2019) e1805121. https://doi.org/10.1002/adma.201805121.
[31] W. Zhao, J. Ding, Y. Zou, C.A. Di, D. Zhu, Chemical doping of organic semiconductors for thermoelectric applications, Chem. Soc. Rev. 49 (2020) 7210-7228. https://doi.org/10.1039/d0cs00204f.
[32] Z. Cai, D. Zhou, M. Wang, S.M. Bak, Y. Wu, Z. Wu, Y. Tian, X. Xiong, Y. Li, W. Liu, S. Siahrostami, Y. Kuang, X.Q. Yang, H. Duan, Z. Feng, H. Wang, X. Sun, Introducing Fe(2+) into nickel-iron layered double hydroxide: local structure modulated water oxidation activity, Angew. Chem. Int. Ed. 57 (2018) 9392-9396. https://doi.org/10.1002/anie.201804881.

[33] Z. Zheng, D. Wu, G. Chen, N. Zhang, H. Wan, X. Liu, R. Ma, Microcrystallization and lattice contraction of NiFe LDHs for enhancing water electrocatalytic oxidation, Carbon Energy 4 (2022) 901-913. https://doi.org/10.1002/cey2.215.
[34] Y. Hao, Y. Li, J. Wu, L. Meng, J. Wang, C. Jia, T. Liu, X. Yang, Z.P. Liu, M. Gong, Recognition of surface oxygen intermediates on NiFe oxyhydroxide oxygen-evolving catalysts by homogeneous oxidation reactivity, J. Am. Chem. Soc. 143 (2021) 1493-1502. https://doi.org/10.1021/jacs.0c11307.
[35] K. Jiang, M. Luo, M. Peng, Y. Yu, Y.R. Lu, T.S. Chan, P. Liu, F.M.F. de Groot, Y. Tan, Dynamic active-site generation of atomic iridium stabilized on nanoporous metal phosphides for water oxidation, Nat. Commun. 11 (2020) 2701. https://doi.org/10.1038/s41467-020-16558-1.
[36] F. Dionigi, J. Zhu, Z. Zeng, T. Merzdorf, H. Sarodnik, M. Gliech, L. Pan, W.X. Li, J. Greeley, P. Strasser, Intrinsic electrocatalytic activity for oxygen evolution of crystalline 3d-transition metal layered double hydroxides, Angew. Chem. Int. Ed. 60 (2021) 14446-14457. https://doi.org/10.1002/anie.202100631.
[37] L. Tao, Y. Yang, H. Wang, Y. Zheng, H. Hao, W. Song, J. Shi, M. Huang, D. Mitlin, Sulfur-nitrogen rich carbon as stable high capacity potassium ion battery anode: Performance and storage mechanisms, Energy Stor. Mater. 27 (2020) 212-225. https://doi.org/10.1016/j.ensm.2020.02.004.
[38] Y. Bai, Y. Wu, X. Zhou, Y. Ye, K. Nie, J. Wang, M. Xie, Z. Zhang, Z. Liu, T. Cheng, C. Gao, Promoting nickel oxidation state transitions in single-layer NiFeB hydroxide nanosheets for efficient oxygen evolution, Nat. Commun. 13 (2022) 6094. https://doi.org/10.1038/s41467-022-33846-0.
[39] Q. He, Y. Wan, H. Jiang, Z. Pan, C. Wu, M. Wang, X. Wu, B. Ye, P.M. Ajayan, L. Song, Nickel vacancies boost reconstruction in nickel hydroxide electrocatalyst, ACS Energy Lett. 3 (2018) 1373-1380. https://doi.org/10.1021/acsenergylett.8b00515.